Modeling the transition between orbital and contact phase in rendezvous and proximity operations

Modeling the transition between orbital and contact phase in rendezvous and proximity operations

Erica Scantamburlo
Department of Mechanical and Aerospace Engineering
Politecnico di Torino
Torino, Italy
erica.scantamburlo@polito.it
ORCID: 0000-0003-1556-1102

Martina Ferrauto
Department of Mechanical and Aerospace Engineering
Politecnico di Torino
Torino , Italy
martina.ferrauto@polito.it
ORCID:0009-0001-0942-0058

Davide Sorli
Department of Mechanical and Aerospace Engineering
Politecnico di Torino
Torino , Italy
davide.sorli@polito.it

Stefano Mauro
Department of Mechanical and Aerospace Engineering
Politecnico di Torino
Torino , Italy
stefano.mauro@polito.it

***Abstract*— Carrying out proximity operations in Earth or Moon orbit during which a capture or docking operation is forecast requires a strong effort in mission planning in order to complete the approach manoeuver and to manage the complex phase of capture. A complete digital twin of all the satellites and bodies involved in the maneuver can provide a useful tool to design the controllers and to test preliminarily possible options and solutions. Within the MUSAPOEM project this kind of tool is under development. It considers the approach phase and a berthing manoeuver, proposing a set of models conveniently related one to each other in order to simulate the different phases of the mission: far approach, short range approach and berthing.**

Keywords*— *Rendezvous and Proximity operations, contact dynamics, orbital dynamics, MUSAPOEM

I. Introduction

In the last years, a lot of attention has been dedicated to the design of novel and innovative concepts of operation for proximity operations, such as rendezvous, docking, berthing of two (or more satellites) that are orbiting the Earth or the Moon. In particular, the interest of space agencies in rendezvous and proximity operations (RPOs) is increasing since the possibility to develop autonomous and automated guidance, navigation and control (GN&C) algorithms for in-orbit operations that lead to extending the operational lifetime of artificial satellites. One of the main objectives of RPOs entailing the operational lifetime of space missions is on-orbit servicing without the presence of humans, such as the repairing and refueling of artificial satellites equipped with a docking and/or robotic manipulators system. Examples of space mission designed for on-orbit servicing are *Orbital Express* (2007) and *Mission Extension Vehicle (first launch in 2019)*.

For RPOs involving two satellites, a controlled satellite, called chaser, that approaches another satellite through the application of GN&C algorithms. The latter satellite is called target, and it can be cooperative or non-cooperative.

During a RPO, it is chosen to divide the interaction between the satellites into two distinct phases depending on their relative distance: the *orbital phase* (OP), and the *contact phase* (CP). In the OP, the motion of satellites is governed by the classical gravitational Newton law. In particular, it is assumed that no mutual interactions exist between the satellites involved, and that the motion of the satellites is only affected by one primary (for example, the Earth). The investigation of the relative motion with the presence of only one gravitational attractor has been widely investigated. In particular, when the target is performing a circular orbit, the linearized equations of motion governing the relative motion of the chaser with respect to the target are known as Hill-Clohessy-Wiltshire equations. When the target is performing an elliptical orbit, the linearized equations of motion describing the relative dynamics are called Tschauner-Hempel equations, and are periodic in the target true anomaly. A derivation of the analytical solution of the Tschauner-Hempel equations is proposed in [1]. Conversely, in the CP the satellites are treated as a single multi-body system, whose dynamics is governed by the mechanical interactions between the end-effector of the chaser robotic system and the target satellite. The transition from the OP to the CP (or from the CP to OP, if a separation operation is considered) leads to discontinuity in the model, that occurs when the relative distance between the chaser and the target is smaller than a threshold value ε. The parameter ε depends on the properties of the chaser robotic system.

The establishment of a mechanical connection between a servicer satellite and its target is fundamental for OOS missions. This connection can be realized through docking or berthing [2]. Berthing, in particular, requires an assisted or semi-autonomous process where the servicer, guided by its GNC system, maneuvers into a precise rendezvous position. A robotic manipulator—mounted on either the chaser or the target—then captures and aligns the two satellites at the designated interface. Throughout this process, the servicer's GNC ensures an appropriate relative positioning, characterized by a specific pose and minimal relative velocity [3].

During CP, the interaction between the chaser and the target shifts from orbital dynamics to physical contact, where the end-effector establishes a controlled grasp on the target. The forces exchanged at the gripping interface are influenced by factors such as actuation torque, friction and potential misalignments. The gripper mechanism must provide a stable grip while minimizing impact forces that could lead to structural damage. Accurate modelling of these interactions is essential for predicting system response and designing control strategies that ensure successful berthing operations.

Space robotic systems play a crucial role in these operations. Typically, such systems comprise a servicing spacecraft, a robotic arm with multiple degrees of freedom (DOF), and the target satellite [4]. One of the earliest examples of space manipulators was the Canadarm-1, first

deployed during NASA's STS-2 mission in 1981 [5]. This success led to the development of Canadarm-2, which has been operational on the International Space Station (ISS) since 2001 and introduced redundancy with its seven-DOF design [6]. In recent years, other space agencies have contributed their own robotic systems. ESA's European Robotic Arm (ERA), featuring a seven-DOF structure and modular end-effectors, enhances handling flexibility [7], while the JEM Remote Manipulation System, developed by JAXA, is specifically designed to support experimental operations aboard the Japanese Experiment Module [8].

The effectiveness of robotic arms in space servicing has been demonstrated through multiple missions, including Hubble Space Telescope maintenance and ISS assembly tasks [9]. More recently, efforts have been directed toward autonomous OOS capabilities. NASA's OSAM-1 mission is set to validate in-orbit assembly using the SPIDER robotic arm, aimed at constructing a satellite communication antenna [10]. The mission underwent a critical review in 2022 and was independently assessed in 2024 [11]. In contrast, the OSAM-2 mission, initially conceived for in-orbit manufacturing with a seven-DOF robotic arm developed by Motiv Space Systems [12], was ultimately canceled in September 2023 due to budget constraints and schedule delays [13].

An emerging field within space robotics is active debris removal (ADR). A notable proposal in this area is the POPUP soft robotic arm, initially designed for debris capture [14] and later adapted for additional onboard applications [15]. One of the critical challenges in berthing operations is the interaction between the robotic end-effector and the target satellite, as the contact forces introduce disturbances to the servicer's GNC system [16]. The behavior of space manipulators and their targets can be analyzed through Kane's equations, which describe the dynamics under free-floating conditions by neglecting gravitational and celestial mechanics influences [17].

The correct identification of the transition between the two phases is essential for RPO. As a matter of fact, possible approximation transition errors may lead to the failure of the proximity operation, as well as structural damage of the satellites. Furthermore, this examination is relevant also for the development of a digital twin able to perform real time simulations for hardware-in-the-loop testing of on-board computer and sensors.

The paper structure is the following: in Section II it is introduced the equations of motion governing the orbital motion of the chaser satellite in the target local-vertical local-horizontal coordinate system leading the OP. It is also proposed the contact dynamics leading the CP. Then, It is identified an algorithm providing the transition between the OP and CP.

The simulation model captures the multibody dynamics of the chaser and target within the ε threshold, considering both berthing and unberthing maneuvers. During berthing, the robotic arm executes a controlled approach, securely captures the target, and aligns it for docking. In the unberthing phase, the arm detaches, withdraws, and releases the target with minimal trajectory disturbances. The analysis of relative velocity profiles confirms precise control during these operations, ensuring stable and efficient satellite servicing.

II. METHODOLOGY

A. Relative orbital dynamics

Since the relative distance of interest between the two satellites for RPOs ranges from 1 km to a few meters, and since the time duration is of order of one satellite orbital period, It can be assumed that the satellites motion is governed by the Kepler restricted two-body problem.

In particular, it is assumed that the target (P_0) and the chaser (P_1) satellites are orbiting a massive body, called primary (or attractor) with gravitational parameter μ. Let r_0 and r_1 be the position vectors of P_0 and P_1 respectively in an inertial reference frame centered at the attractor. It is supposed that the attractor is a spherical and homogeneous body. In such a way the primary can be modelled as a point mass. Furthermore, because of the time duration of the RPOs, it is considered that the dynamics of both the satellites is well approximated by the Kepler restricted two-body problem, and that no mutual interaction between the satellites occurs. For the design of RPOs, it is useful to introduce the target local-vertical local-horizon (LVLH) frame that is centered at the target position and whose axis $\hat{t_1}$, $\hat{t_2}$, and $\hat{t_3}$ are defined as follows: $\hat{t_1}$ is parallel and directed as the position vector of the target with respect to the attractor, $\hat{t_3}$ is parallel and directed as the angular momentum of the target, and $\hat{t_2}$ is calculated accordingly to the right-hand rule. Then, the relative position of the chaser with respect to the target is defined as $\boldsymbol{\rho}=\boldsymbol{r}_1-\boldsymbol{r}_0$. Let us denote by x, y, and z the components of $\boldsymbol{\rho}$ in the target LVLH. Then, the system of differential equations governing the motion of the chaser satellite with respect to the target in the target LVLH is the following:

$$\ddot{x} - 2\dot{\theta}\dot{y} - \ddot{\theta}y - \dot{\theta}^2 x = -\frac{\mu(|r_0| + x)}{[(|r_0| + x)^2 + y^2 + z^2]^{3/2}} + \frac{\mu}{|r_0|^2} \quad (1)$$

$$\ddot{y} + 2\dot{\theta}\dot{x} + \ddot{\theta}x - \dot{\theta}^2 y = -\frac{\mu\, y}{[(|r_0| + x)^2 + y^2 + z^2]^{3/2}} \quad (2)$$

$$\ddot{z} = -\frac{\mu\, z}{[(|r_0| + x)^2 + y^2 + z^2]^{3/2}} \quad (3)$$

with $|\boldsymbol{r}_0| = a(1-e^2)/(1+e\cos\theta)$, where a, e, and θ denote the semimajor axis, eccentricity and true anomaly of the target satellite respectively, and

$$\dot{\theta} = \sqrt{\frac{\mu}{a^3(1-e^2)^3}}(1+e\cos\theta)^2 \quad (4)$$

It is noticed that the system of equations governing the relative dynamics of the chaser with respect to the target admits an equilibrium at the origin, i.e., at the target position.

To complete a rendezvous, the components of the relative position vector x, y and z must converge to the origin. In literature, there exist several approaches designed for this purpose. For example, a two-impulsive maneuver can be planned, in a way that two instantaneous changes of the chaser velocity guarantee the rendezvous (see, for example, [19,20]); Recently, with the growing interest in the Model Predictive Control (MPC) as class optimal control algorithm (see, for example,[21]), several research works are devoted to the

development of MPC strategies as a tool for autonomous rendezvous [22] [23][24].

B. Contact dynamics

The gripper and interface system is key to the successful execution of berthing maneuvers between the chaser and target satellites. The End-Effector (EE) must apply precise and controlled forces during contact to ensure stable engagement between the satellites while preventing damage or malfunction. The grasping system consists of several mechanical components, including the gripper, actuation mechanisms and motion control systems. The gripper is designed to grip the target interface and apply a normal force to ensure stable contact. This requires a balance between force control and actuation torque.

The EE incorporates gear mechanisms that provide torque control for precise gripping. The gear ratios are optimized to ensure low actuation torque while maintaining grip, allowing efficient, controlled interaction with the target interface.

As shown in Figure 1, the EE consists of two main components: the gripper and the actuation system, which controls its position and movement. The gripper has two fingers designed to ensure a secure and aligned grip on the target interface, preventing misalignment.

Each finger is connected to an actuation system that applies the necessary force for stable contact. Their optimized geometry maximizes the contact area, reducing the risk of slippage or damage.

The actuators are coupled to a gearbox, shown in Figure 1 which transmits torque to the gripper fingers, driving their movement during the berthing process. The gear mechanism of the end-effector is composed of three gears designed to optimize torque transmission while respecting the compact size constraints of the gearbox. This system enables precise control over the clamps' movement during docking, ensuring synchronization and sufficient normal force application to the target interface.

The actuation system of the End-Effector employs a three-gear configuration: *i) Gear 1 (Motor Gear):* Connected to the actuator, this gear has Z_1 teeth and transmits torque to the second gear; *ii) Gear 2 (First Clamp Gear):* This gear has Z_2 teeth and is directly attached to the first clamp. It engages both Gear 1 and Gear 3; *iii) Gear 3 (Second Clamp Gear):* Identical to Gear 2 ($Z_2 = Z_3$), this gear is attached to the second clamp and rotates in synchronization with Gear 2.
The total transmission ratio is determined by the gear pair engagement:

$$R = \frac{\omega_1}{\omega_3} = \frac{Z_2}{Z_1} \tag{5}$$

With $Z_1 = 15$ teeth (Motor Gear) and $Z_2 = Z_3$ teeth (Clamp Gears), the resulting transmission ratio is 2. This ratio ensures that the rotational speed of the clamps is reduced by half while the torque is amplified by a factor of 2, enabling precise force application during docking. The gear teeth have been optimized to minimize backlash and maximize efficiency, contributing to smooth and reliable operation.

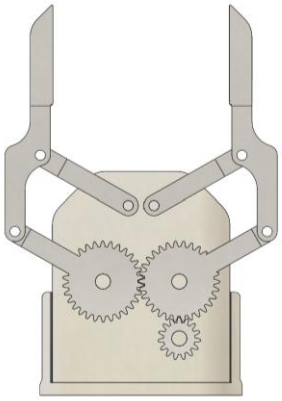

Figure 1, End-Effector concept section.

The gearbox dimensions are carefully designed to fit within the EE's spatial constraints. The arrangement of the three gears and the integration with the actuator ensures that the entire system remains compact without compromising performance. The gearbox dimensions are carefully designed to fit within the EE's spatial constraints. The arrangement of the three gears and the integration with the actuator ensures that the entire system remains compact without compromising performance. The End-Effector's actuation, shown in Figure 2, system can be modeled by the following equations, which relate the motor torque, gear velocities, and the forces applied by the clamps. The velocity at the contact point of the clamps is the same for both clamps:

$$\begin{aligned} v_2 = v_3 = V &= \omega_2 \cdot r \cdot \sin(\gamma) \\ &= \omega_1 \left(\frac{Z_1}{Z_2}\right) \cdot r \cdot \sin(\gamma) \end{aligned} \tag{6}$$

Here, r and γ are the radius and the angle shown in the scheme in Figure 2. The force F acting on the clamp can be related to the torque C_2 on the second gear. The factor of 2 is due to the clamp acting symmetrically on both sides of the contact.

$$C_2 = 2 \cdot F \cdot r \cdot \sin(\gamma) \tag{7}$$

Finally, the contact force F acting on the clamp is directly proportional to the motor torque M_t, with the transmission ratio $\left(\frac{Z_1}{Z_2}\right)$ and the geometry of the system (radius r and angle γ) playing a key role.

$$F = \frac{Z_1}{Z_2} \cdot \frac{1}{2 \cdot r \cdot \sin(\gamma)} \cdot M_t \tag{8}$$

The equations described above establish the relationship between motor torque, gear speeds and the forces acting on the clamps in the end-effector system. By applying these equations it is possible to calculate the force exerted by the clamps and the speed at which the clamps move during the berthing process.

The actuation system allows precise control of the normal force applied by the clamps. By regulating the torque applied to Gear 1, the system ensures that the normal force at the interface meets the requirements for adhesion without exceeding safe limits.

This force regulation is particularly important during dynamic docking scenarios, where excessive forces could lead to misalignment or damage to the target interface.

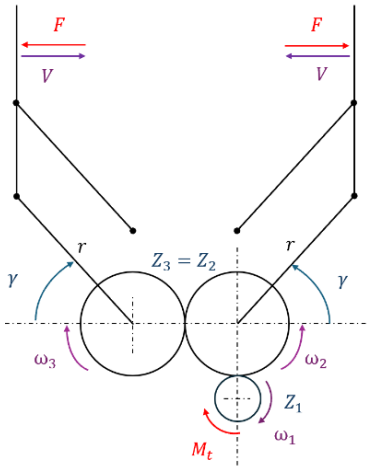

Figure 2, End-effector gearbox diagram.

The actuation system enables precise regulation of the normal force applied by the clamps, ensuring secure contact with the target interface throughout the docking process. The normal force is calculated based on system parameters using the following formula:

$$M_t = m_t \cdot a_0 \cdot b \cdot c_s/(2 \cdot \mu_d) \quad (9)$$

$$F = 2 \cdot M_t/(8 \cdot b) \quad (10)$$

where m_t is the target mass, a_0 is the maximum acceleration of the end-effector, b is the contact area width of the clam, c_s is the safety coefficient, accounting for variations in contact conditions, μ_d is the dynamic friction coefficient, M_t is the torque transmitted to the clamps and F is the total normal force applied by the clamps.

The equation (9) determines the torque required to achieve the desired force at the interface, factoring in the target mass and friction conditions. The equation (10) translates this torque into the normal force distributed across the clamps.

To ensure reliable operation, the system implements a strategy (shown in Figure 3) that maintains consistent grip pressure even during transient contact conditions. The process begins with a Contact Trigger, which indicates the initial condition where the system detects a possible interaction (this trigger can be either 0 or 1).

The contact signal itself is delayed and a sample and hold mechanism is used to capture the state of the contact signal at the appropriate time just before the actual engagement occurs. This ensures that the system responds at the precise moment when the gripper is about to contact the workpiece, preventing premature force application.

The EE pick and place trigger signal is then determined by comparing the position and orientation error signals. The system evaluates two critical errors: *i) Position Error*: the magnitude of the positional deviation is computed as the Euclidean norm of the positional components dx, dy, dz. If this magnitude is below a threshold (e.g., 2×10^{-3} $[m]$), the position trigger increments: $trigger = min(trigger + 1,1)$. This ensures that the trigger saturates at 1. *ii) Orientation Error*: similarly, the magnitude of the orientation deviation is evaluated. If it falls below a threshold (e.g., 1×10^{-3} $[rad]$), the orientation trigger increments using the same logic: $trigger = min(trigger + 1,1)$.

Both conditions are evaluated separately in their respective Simulink subsystems. Each subsystem outputs its individual trigger value. The two trigger values (one for position and one for orientation) are then passed to a MIN block. This block ensures that the system responds to the most critical constraint by selecting the minimum trigger value.

This strategy guarantees that the end-effector only proceeds when both constraints (position and orientation) are satisfied. After the triggers are combined, the resulting value (Pick-Place Trigger) is compared against a threshold of 0.5: *i)* $If\ Pick - Place\ Trigger > 0.5$: This indicates that both position and orientation are sufficiently accurate. At this point, the system activates the torque for the end-effector (e.g., $Torque = Mt$). *ii)* If $Pick - Place\ Trigger <= 0.5$: The torque remains at zero (Torque = 0), ensuring that no premature engagement occurs.

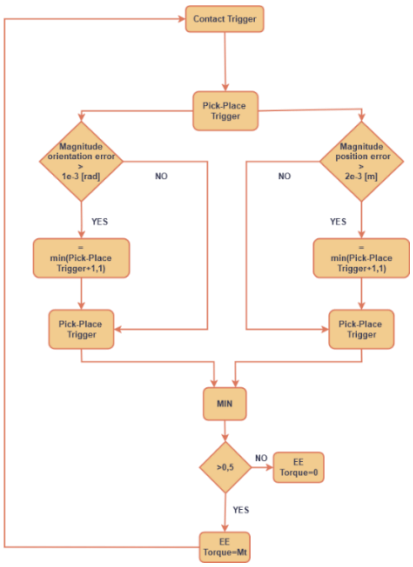

Figure 3, Grasping algorithm

C. *Interface scheme for the transition between orbital to contact dynamics*

In spacecraft docking operations, the interaction between a chaser and a target spacecraft is divided into different phases based on their relative distance. As shown in the flowchart in Figure 4 when the distance between the chaser and the target is greater than a critical threshold ε, the orbital dynamics of the two spacecraft is considered in order to model their trajectories.

At this stage, the chaser-target system is treated as a single multibody system, with the dynamics focusing on the interaction between the chaser's end-effector and the target. This simplification is justified because at short distances the gravitational interaction between the attractor (for example, the Earth or the Moon) and the satellites become negligible. The flowchart in Figure 4 also distinguishes between two outcomes: if the chaser's end-effector has already contacted

the target, the operation is classified as "unberthing". If contact has not yet occurred, the simulation focuses on completing the "berthing" maneuver.

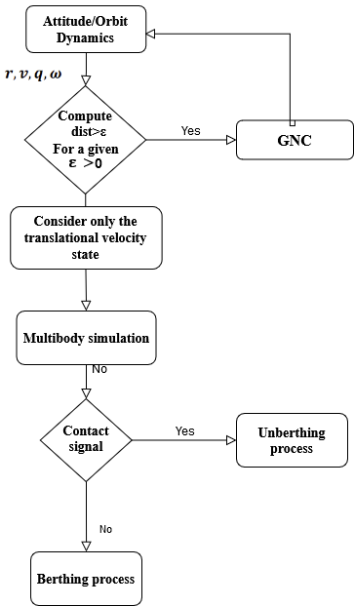

Figure 4, Transition from orbital dynamics to relative motion modeling based on distance.

The transition from orbital dynamics to relative motion modeling is clarified in Figure 5 in which the exchange of velocities and orientations between the two models is emphasized. Before reaching the threshold ε, the orbital dynamics model governs the motion of both spacecraft. Once the chaser enters the critical region (defined by the threshold value ϵ), the multibody model takes over, focusing on the translational dynamics of the chaser-target system.

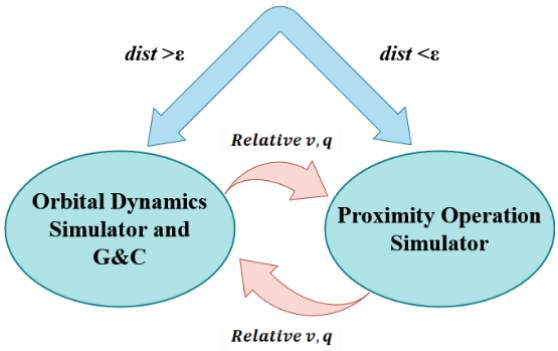

Figure 5, Velocity and orientation exchange between models

At the initial time t_0, the chaser's relative position and velocity state in the target LVLH are $\boldsymbol{r_0} = (x_0, y_0, z_0)^T$ and $\boldsymbol{v_0} = (v_{x0}, v_{y0}, v_{z0})^T$. If the distance between the center of the mass of the chaser and the target is larger than a given threshold value ε (whose value is set equal to 3,603 $[m]$, based on the robotic arm's dimensions relative to the satellites' size, ensuring target capture without singularity issues as the target stays within the workspace) the system of equations reported in (3) is numerically propagated.

Generally, to start proximity operation, guidance and control algorithms are integrated, as the aim is to maneuver the chaser closer to the target. For this reason, at each integration step, the dynamics and the G&C algorithms are integrated until the distance between the chaser and the target is smaller than the threshold value ε.

III. Results

The simulation model captures the multibody dynamics between the chaser and the target within the ε distance threshold. The system has a reference frame fixed to the target spacecraft, with the chaser's position and velocity defined relative to this frame. The multi-body model includes the dynamics of the chaser's robotic arm, its end effector and any physical interactions with the target during docking and undocking operations. Depending on the operation, the simulation distinguishes two key phases: *i)* Berthing, where the robotic arm captures and secures the target; *ii)* Unberthing, where the robotic arm detaches from the target to release it.

A. Berthing Maneuver

The berthing process, as shown in Figure 6, involves three phases: *i) Approach phase*: The robotic arm moves towards the target, aligning the end-effector with the docking point. During this phase, the Guidance, Navigation and Control (GNC) system ensures accurate positioning, while the robotic arm minimizes residual misalignment; *ii) Capture phase:* The end-effector makes contact with the target interface and applies controlled forces to secure the connection. The gripper-type end effector designed for this task ensures stability by maintaining parallelism and sufficient friction for adhesion. Simplified contact proxies (e.g. sphere-plane contact) optimize computational efficiency; *iii) Docking phase*: Once the target is secured, the robotic arm adjusts to align the spacecraft's docking ports, completing the mechanical coupling.

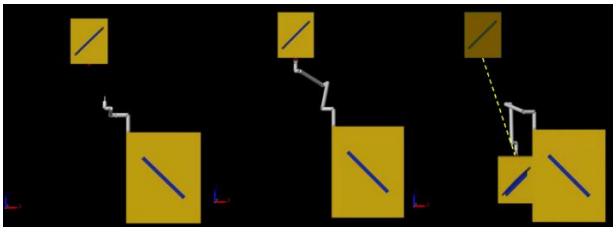

Figure 6, Berthing phases.

The relative velocity profiles are analyzed and presented in Figure 7 to better illustrate this dynamic process. The graphs of relative velocities along the x, y and z axes highlight the controlled deceleration and trajectory adjustments required for alignment.

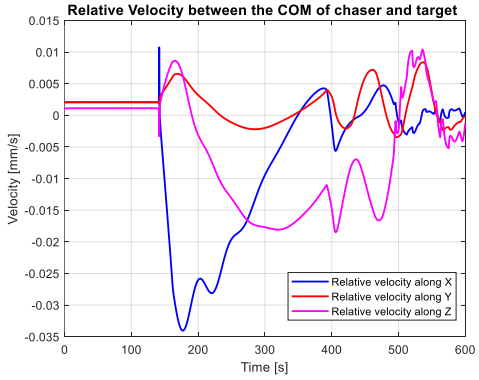

Figure 7, Relative velocities during berthing process.

B. *Unberthing Maneuver*

The unberthing operation reverses the steps of the berthing process, detailed in Figure 8:*i) Grasping from Operational Position*: The robotic arm secures the target spacecraft from its operational position, establishing a rigid connection; *ii) Arm Deployment and Withdrawal*: The robotic arm carefully extends, moving the target away from its initial position in a controlled manner to avoid disturbances; *iii) Release at Designated Position*: The arm positions the target at a predefined location and releases it, ensuring minimal disturbance to its trajectory.

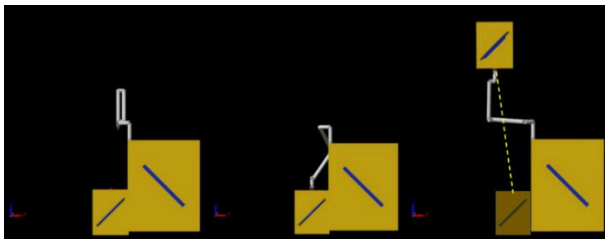

Figure 8, Unberthing phases

The relative velocity plots along the x, y and z axes shown in Figure 9 are crucial for analyzing the unberthing process. They show the increase in relative velocities as the chaser carefully moves the target away from the operational interface.

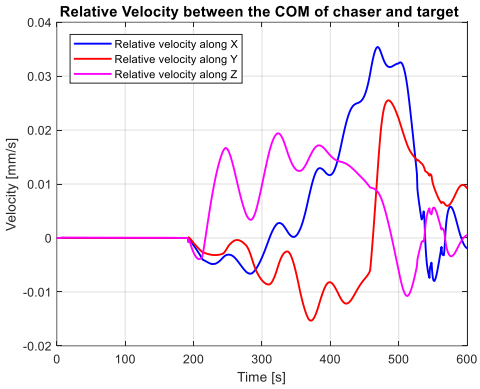

Figure 9, Relative velocities during unberthing process

ACKNOWLEDGMENT

This research is coordinated and funded by the Italian Space Agency (Agenzia Spaziale Italiana, ASI) in the framework of the RESEARCH DAY "GIORNATE DELLA RICERCA ACCADEMICA SPAZIALE" initiative through the contract no. ASI-BVTECH-2023-2-E.0
The authors thank ASI for its support and coordination.

REFERENCES

[1] Yamanaka K., and Ankersen F., "New state transition matrix for relative motion on an arbitrary elliptical orbit", Journal of Guidance, Control, and Dynamics, Vol.25, No. 1, 2002

[2] E. Papadopoulos, F. Aghili, O. Ma, and R. Lampariello, "Robotic Manipulation and Capture in Space: A Survey," *Frontiers in Robotics and AI*, vol. 8. Frontiers Media S.A., Jul. 19, 2021. doi: 10.3389/frobt.2021.686723.

[3] A. Flores-Abad, O. Ma, K. Pham, and S. Ulrich, "A review of space robotics technologies for on-orbit servicing," *Progress in Aerospace Sciences*, vol. 68. Elsevier Ltd, pp. 1–26, 2014. doi: 10.1016/j.paerosci.2014.03.002.

[4] Canadian Space Agency, "About Canadarm," https://www.asc-csa.gc.ca/eng/ canadarm/about.asp.

[5] Canadian Space Agency, "About Canadarm 2," https://www.asc-csa.gc.ca/eng/ iss/canadarm2/about.asp.

[6] European Space Agency, "European Robotic Arm," https://www.esa.int/Science_Exploration/Human_and_Robotic_Exploration/International_Space_Station/European_Robotic_Arm.

[7] P. Laryssa et al., "International Space Station Robotics: A Comparative Study of ERA, JEMRMS and MSS."

[8] B. Franklin, "On-Orbit Satellite Servicing Study Project Report 'Energy and persistence conquer all things.,'" 2010.

[9] D. Arney, J. Mulvaney, C. Williams, R. Sutherland, and C. Stockdale, "In-space Servicing, Assembly, and Manufacturing (ISAM) State of Play 2022 Edition."

[10] NASA, "OSAM-1 Mission," https://www.nasa.gov/mission/on-orbit-servicing-assembly-and-manufacturing-1/.

[11] NASA's Goddard Space Flight Center, "NASA's Robotic OSAM-1 Mission," https://www.nasa.gov/centers-and-facilities/goddard/nasas-robotic-osam-1-mission-completes-its-critical-design-review/.

[12] "FINAL REPORT OF THE OSAM-1 INDEPENDENT REVIEW BOARD 29 FEBRUARY 2024 Background." [Online]. Available: https://sed.gsfc.nasa.gov/etd/583/tech/asist.

[13] NASA, "OSAM-2 Mission," https://www.nasa.gov/mission/on-orbit-servicing-assembly-and-manufacturing-2-osam-2/.

[14] E. Tunstel, C. Thayer, B. Hayashi, and R. Saltus, "ModuLink: A Robotic Manipulation Applique for In-Space Servicing Vehicles," in IEEE Aerospace Conference Proceedings, IEEE Computer Society, 2023. doi: 10.1109/AERO55745.2023.10115712.

[15] P. Palmieri, M. Gaidano, M. Troise, L. Salamina, A. Ruggeri, and S. Mauro, "A deployable and inflatable robotic arm concept for aerospace applications," in 2021 IEEE International Workshop on Metrology for AeroSpace, MetroAeroSpace 2021 - Proceedings, Institute of Electrical and Electronics Engineers Inc., Jun. 2021, pp. 453–458. doi: 10.1109/MetroAeroSpace51421.2021.9511654.

[16] P. Palmieri, M. Gaidano, A. Ruggeri, L. Salamina, M. Troise, and S. Mauro, "An Inflatable Robotic Assistant for Onboard Applications," in Proceedings of the International Astronautical Congress, IAC, International Astronautical Federation, IAF, 2021.

[17] X. L. Ding, Y. C. Wang, Y. B. Wang, and K. Xu, "A review of structures, verification, and calibration technologies of space robotic systems for on-orbit servicing," Science China Technological Sciences, vol. 64, no. 3. Springer Verlag, pp. 462–480, Mar. 01, 2021. doi: 10.1007/s11431-020-1737-4.

[18] S. Wu, F. Mou, Q. Liu, and J. Cheng, "Contact dynamics and control of a space robot capturing a tumbling

[19] Alfriend K.T., Vadali S.R., Gurfil P., How J.P. and Breger L.S., "Spacecraft Formation Flying. Dynamics, control and navigation". Butterworth-Heinemann, 2010

[20] Battin R.H., "An Introduction to the Mathematics and Methods of Astrodynamics", AIAA, 1999

[21] Rawling J.B., Mayne D.Q., and Diehl M.M., "Model Predictive Control", Nob Hill Pub, 2009

[22] Salzo F.P., Bucchioni G., and Vazquez R., "Design of a Model Predictive Controller for formation flight on quasi-Halo orbit", Proceedings of the 2024 CEAS EuroGNC conference, 2024

[23] Pagone M., Bucchioni G., Alfino F., and Novara C., "Autonomous Lunar rendezvous trajectory planning and control using nonlinear MPC and Pontryagin's principle", IFAC Journal of Systems and Control, 2024

[24] Pilone F., Bucchioni G., Boone S., Lizy-Destrez S., "Autonomous mission planning for multi-agent Lunar mission", Proceedings of the International Astronautical Congress, 2024